

# Theory of interacting dislocations on cylinders

Ariel Amir,<sup>1</sup> Jayson Paulose,<sup>2</sup> and David R. Nelson<sup>1</sup>

<sup>1</sup>*Department of Physics, Harvard University, Cambridge, MA 02138, USA*

<sup>2</sup>*Harvard School of Engineering and Applied Sciences, Cambridge, MA 02138, USA*

We study the mechanics and statistical physics of dislocations interacting on cylinders, motivated by the elongation of rod-shaped bacterial cell walls and cylindrical assemblies of colloidal particles subject to external stresses. The interaction energy and forces between dislocations are solved analytically, and analyzed asymptotically. The results of continuum elastic theory agree well with numerical simulations on finite lattices even for relatively small systems. Isolated dislocations on a cylinder act like grain boundaries. With colloidal crystals in mind, we show that saddle points are created by a Peach-Koehler force on the dislocations in the circumferential direction, causing dislocation pairs to unbind. The thermal nucleation rate of dislocation unbinding is calculated, for an arbitrary mobility tensor and external stress, including the case of a twist-induced Peach-Koehler force along the cylinder axis. Surprisingly rich phenomena arise for dislocations on cylinders, despite their vanishing Gaussian curvature.

PACS numbers: 61.72.Lk, 05.10.Gg, 61.72.Yx 64.60.Qb 87.10.-e

## INTRODUCTION

Defects in crystals such as dislocations have been studied extensively for more than seven decades [1–3], and their importance in condensed matter physics and material science is widely recognized [4]. Systems of dislocations in both two and three dimensions can be realized experimentally. Mechanical properties of bulk metals are strongly affected by the dynamics of dislocation lines within them [4], and two-stage melting of a two-dimensional crystal can be driven by dislocations [5]. Interesting applications involve a two dimensional particle array with a periodic boundary conditions in one direction: a cylindrical crystal. One such example involves interacting colloids on the surface of a liquid film coating a solid cylinder, where repulsive forces give rise to the self-organized emergence of a two dimensional crystalline solid. Defects in colloidal assemblies on the related curved surfaces of capillary bridges were recently studied experimentally and theoretically [6]. Here, the Gaussian curvature can be positive or negative; the zero Gaussian curvature of a cylinder is a special case [7]. The growth of the cell walls of rod-shaped bacteria provides a biophysical example. Their geometry can be approximately described by a cylinder, and in a recent study [8, 9] we have argued that one may regard cell wall elongation as mediated by dislocation climb [4]. As a final motivation we note that the hydrodynamic interactions of vortices on cylinders is mathematically similar to those of dislocations, albeit simpler since in this case the bare interactions on a flat surface are isotropic [10]. Vortices on superfluid Helium films were studied in a cylindrical geometry, in order to model superfluids in porous materials [11]. A type II superconducting, hollow wire could have similar interacting vortices on its cylindrical surface.

Fig. (1) illustrates the simplest dislocation in two-dimensional square and triangular lattices. For the

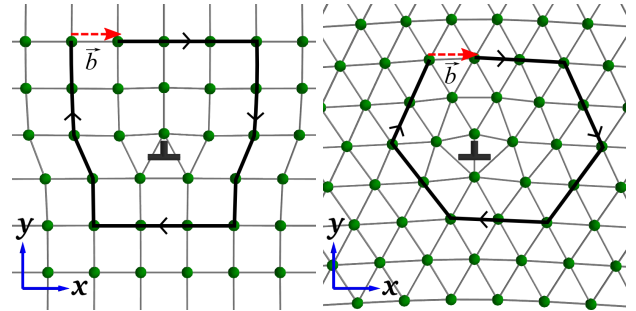


FIG. 1. Lattice configuration corresponding to a single dislocation with Burgers vector in the positive  $x$  direction for a square (left) and triangular (right) lattice of masses and harmonic springs relaxed to their equilibrium configuration. The Burgers vector is defined as the deficit (red arrow) of a clockwise loop that would be closed in the absence of a dislocation; hence  $\vec{b} = b\hat{x}$  in both cases, where  $b$  is the lattice constant. The ‘T’ symbol encodes both the position and orientation of the dislocation; the leg of the inverted ‘T’ points in the direction of added material.

square lattice, the dislocation can be thought of as the termination of a semi-infinite row of lattice points added to the upper half of an otherwise perfect lattice. For the triangular lattice, the dislocation represents the termination of *two* semi-infinite rows of particles, inclined at  $\pm 30^\circ$  to the vertical. Generally, the dislocation can be characterized by a topological invariant called the Burgers vector, defined by the Burgers circuit [4],  $\vec{b} = \oint \frac{\partial u}{\partial l} dl$  (see Fig. 1). It is immediately apparent that such defects distort the crystalline lattice in their vicinity. For both the triangular and square lattice, it is possible to associate a particular set of neighbors to each lattice site by assigning near neighbor bonds. This allows us to define the dislocations using the number of neighbors: in the square lattice, the dislocation core has three sites with five nearest neighbors. In the triangular lattice,

the Voronoi construction shows that the dislocation is characterized by a five-fold site (a site with five nearest neighbors) bonded to a seven-fold site.

The structure of the manuscript is as follows. We first describe two scenarios, one motivated by cell wall growth of rod-shaped bacteria and the other by colloidal crystals on cylinders, and show that they require understanding the dynamics of interacting dislocations on a rectangular and triangular lattice, respectively. In contrast to the predominantly climb dislocation dynamics relevant to elongating bacteria [9], the dynamics appropriate to colloidal assemblies on cylinders is predominantly glide, *i.e.*, the motion is parallel as opposed to perpendicular to the Burgers vector [4]. We analyze the form of the interactions between dislocations with arbitrary Burgers vector and compare the results to numerical simulations showing that, surprisingly, good agreement with continuum elastic theory is already achieved for relatively small systems. We then proceed to exploit a useful connection between isolated dislocations on a cylinder and the physics of grain boundaries. Finally, we discuss related ‘nucleation’ problems: Upon the addition of a force in the circumferential direction driving defects of opposite sign apart, there will be a finite unbinding rate at non-zero temperature. We calculate this rate using Langer’s generalization of Kramers’ theory [12, 13], and find interesting geometrical effects associated with the cylindrical geometry. We also discuss the effect of a twisting stress applied to the ends of a cylinder coated with colloids; in this case the strain is relaxed by dislocation pairs separating predominantly along the cylinder axis. The Airy stress function for a dislocation on a cylinder is calculated in Appendix A. In Appendix B, we discuss some subtle aspects of the quantization of stresses and strains on a cylinder, due to periodic boundary conditions.

### Bacterial cell wall growth

Bacterial cell walls are made of a partly ordered mesh of peptidoglycan [14], which can be only a single molecule layer thick in gram-negative bacteria. While there are still many open questions regarding architecture and growth, this meshwork is known to consist of circumferential glycan strands cross-linked by peptides, as shown schematically in Fig. 2. We note that rod-shaped bacteria with very large aspect ratios can be created by suppressing the septation process associated with cell division [15]. To insert new material into the structure, defects in the mesh have to be created. Inserting a single glycan strand between two existing ones would not preserve the topology of the network. However, inserting *two* glycan strands between two existing ones does preserve the topology. This observation has led to the “three-for-one” hypothesis, see for example Ref [16], or, alternatively, the more symmetric process shown in Fig. 2. Each

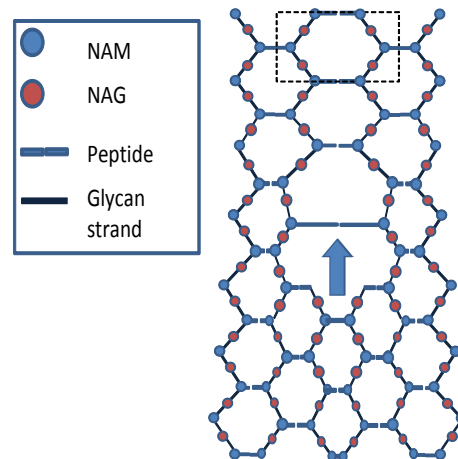


FIG. 2. Schematic illustration of insertions of new glycan strands into the peptidoglycan mesh of a bacterial cell wall. The new material is inserted in the vicinity of the blue arrow, which points azimuthally around the cylinder and sits near the core of the dislocation. The axis of the cylinder runs horizontally, which is also the direction of the Burgers vector of this dislocation. Although the region around the new insertions is distorted, the connectivity of the structure is preserved locally due to the simultaneous insertions of *two* extra glycan strands into the structure, respecting the lattice geometry. The rectangular (dashed-line) box shows the biologically relevant unit cell, which is however not the minimal unit cell of the underlying lattice [8].

zig-zag glycan strand is composed of alternating sugar units called NAM (N-acetylmuramic acid) and NAG (N-acetylglucosamine). For the unit cell shown in Fig. 2, inserting two glycan strands is equivalent to the addition of a single additional unit cell. The coarse-grained lattice obtained in this way is rectangular, and the dislocation can be mediated by edge dislocations climbing in this lattice in the circumferential direction. The relevant Burgers vectors point in the direction of the cylinders axis of symmetry [8, 9].

Here, we shall simplify the analysis by neglecting the anisotropy associated with the two-dimensional rectangular lattice, which would require a non-isotropic elasticity theory with four elastic coefficients to describe elastic deformations of the structure [17]. Rather, we shall approximate the systems’ free energy by the standard isotropic form [18]:

$$F_{elastic} = \int \left[ \frac{\lambda}{2} u_{ii}^2(\vec{x}) + \mu u_{ij}^2(\vec{x}) \right] d^2 x_k, \quad (1)$$

where  $u_{ij}(\vec{x}) = \frac{1}{2} [\partial_i u_j(\vec{x}) + \partial_j u_i(\vec{x})]$  is the 2d strain tensor.  $\lambda$  and  $\mu$  are the two-dimensional *Lam coefficients*. Fig. 3 shows a number of dislocations in a square lattice. Dislocation climb, mediated by glycan strand extension machinery, can be affected by interactions between these dislocations.

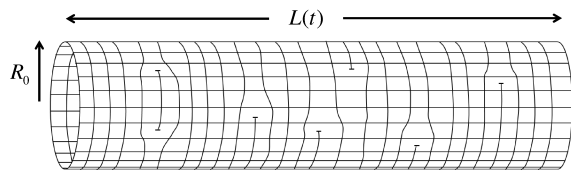


FIG. 3. Schematic of dislocations (i.e. glycan strand ends) on the cylindrical portion of a bacterial cell wall of radius  $R_0$ . A subset of these defects rotate circumferentially when propelled by the addition of material from inside the bacterium, mediated by strand elongation machinery on the dislocation cores (not shown). Constant velocity climb motion of such dislocations leads to exponential elongation of the cylinder length  $L(t)$ ; see Refs. [8, 9].

### Colloidal crystals

Recent experimental advances allow the creation of dislocations in colloidal assemblies with fascinating interfacial geometries, allowing study of the interplay of geometry, including Gaussian curvature, with defects in the lattice structure [6, 19]. In this case the lattice of colloidal particles is typically triangular, with lattice vectors that interact only weakly with the directions of principal curvature. Upon approximating the pair interaction between colloids as harmonic with spring constant  $k_s$  for small displacements about the equilibrium positions, the lattice can be described elastically with isotropic effective Lam coefficients  $\lambda = \mu = \sqrt{3}k_s/4$  [20]. Fig. (1) shows an example of a single dislocation in a triangular lattice. As we shall show here, even in the absence of Gaussian curvature, the periodic boundary conditions associated with a cylindrical geometry give rise to novel phenomena, not found in an infinite plane (to be referred to as “flat space” in the following). In flat space, rotational invariance allows an arbitrary orientation of the crystallographic axis. On a cylinder, however, square and triangular lattices can have an energetically preferred orientation relative to the long axis of the cylinder [21]. With bacterial cell walls, for example, it may be easier to bend the glycan strands than the alternating amino acid cross-bridges, which would lead to a preferred orientation on a cylinder. In this paper, we shall focus primarily on triangular lattices with Bragg rows that run either azimuthally or along the cylinder axis.

### Phyllotaxis

In various biological as well as non-living systems, subunits are arranged in an ordered lattice, wrapped on a cylinder, a particular case of a phenomenon known as *phyllotaxis* (meaning “leaf arrangement” in ancient Greek). These range from plants [22, 23], rod-shaped

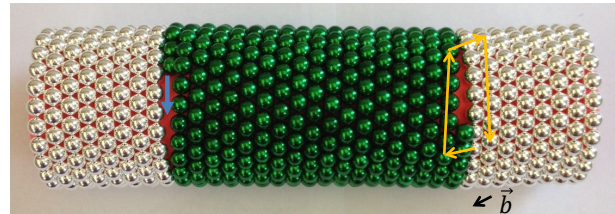


FIG. 4. Model of a dislocation pair on a cylinder. This structure can systematically elongate if new particles (green) are added by two counter-rotating dislocations moving via climb. For one of the dislocations, the climb direction is indicated by a blue arrow. For the other, the Burgers circuit around the dislocation is shown (yellow) as well as the resulting Burgers vector  $\vec{b}$ . Alternatively, the dislocation pair could separate by glide (motion parallel to  $\vec{b}$ ), with motion predominately along the cylinder, with negligible elongation. In both cases, however, a triangular lattice with slightly tilted Bragg rows is created in the center, relative to the purely azimuthal Bragg rows made of silver particles on the two sides. Although the model was constructed with magnetic beads interacting via dipole-dipole interactions, we expect similar configurations for micron-sized colloids assembled on a cylindrical substrate.

viruses and bacterial flagella [24–26] to systems where subunits arrange via magnetic interactions [27–29]. Each phyllotactic arrangement can be characterized by two integers  $(M, N)$ , such that  $Mb\hat{e}_1 + Nb\hat{e}_2 = W\hat{y}$ , with  $\hat{e}_1$  and  $\hat{e}_2$  the two lattice vectors of the triangular lattice, forming a  $60^\circ$  angle between them, and  $\hat{y}$  points in the azimuthal direction around the cylinder of circumference  $W = 2\pi R$ . Such tessellations were recently found useful also in the context of the Thompson problem on a cylinder, *i.e.*, how colloids pack in the bulk of a cylinder [30]. In various scenarios the energetically preferred tessellation can depend on certain external conditions [31, 32], and it is interesting to understand the dynamics of the process through which this change comes about. It is plausible that the boundary region between two competing phyllotactic tessellations will consist of one or several dislocations, see for example Fig 4; as we shall show in section , a dislocation on a cylinder is equivalent to a grain boundary. As an example, Ref [26] suggests that such a change in the phyllotactic arrangement of the tail-sheath of the bacteriophage T4 is driven by 6 dislocations symmetrically arranged on the circumference of the cylinder. These observations provide additional motivation for understanding the interactions between dislocations on a cylinder, which is a necessary step to quantify the “dynamical phyllotaxis” problem sketched above.

### INTERACTING DISLOCATIONS

Consider an edge dislocation on the surface of a cylinder, with radius  $R$  and infinite length. We denote the coordinate along the symmetry axis by  $x$ , and the other

by  $y$ , so that  $y$  is periodic with a period of  $W \equiv 2\pi R$ . For simplicity, and without loss of generality, let us define the axes' origin at the dislocation core. In Ref. [9], some of the components of the stress tensor produced by edge dislocation with Burgers vector  $\vec{b} = \pm b\hat{x}$  were evaluated. Here, we shall calculate all components of the stress produced by dislocations with a Burgers vector  $\vec{b}$  either in the  $\pm b\hat{x}$  or  $\pm b\hat{y}$  direction. For a lattice of any symmetry or orientation with respect to the cylinder axis we could always decompose the dislocation's Burgers vector into two orthogonal components in these directions. Within linear elasticity (and assuming isotropic elastic constants) one could thus use the results presented below to find the stress field induced by a dislocation with a Burgers vector of arbitrary orientation.

In flat space, one may consider a *single* dislocation in an otherwise perfect crystal, in which case the energy of the system diverges logarithmically with the system size. However, the energy of a single dislocation on a long cylinder of length  $L$ , in general diverges as the area  $WL$ , as the subsequent discussion of long-range strains will make clear. An important special case is a Burgers vector in the  $\hat{x}$  direction, when the divergence is only logarithmic in  $W$  and independent of  $L$ . In the case of multiple dislocations on a cylinder, the energy can be decomposed into the divergent terms mentioned above, as well as the interaction energies. In the following, we focus on these pairwise interactions, for two generic Burgers vectors. For configurations where the sum of Burgers vectors vanish (such as cylinders with periodic boundary conditions along the cylinder axis) the divergences discussed above will cancel.

As noted in Ref. [9], the Laplacian on a cylinder is equivalent to that in an infinite two-dimensional flat space together with the periodicity requirement. We exploit this idea by first considering the stresses without the periodicity requirement. Up to a sign depending on the direction of the Burgers vector  $\vec{b} = \pm b\hat{x}$ , the results for the infinite flat space are given by [4]:

$$\sigma_{xx}^{flat} = -Aby(3x^2 + y^2)/r^4, \quad (2)$$

$$\sigma_{yy}^{flat} = Aby(x^2 - y^2)/r^4, \quad (3)$$

and

$$\sigma_{xy}^{flat} = Abx(x^2 - y^2)/r^4, \quad (4)$$

with  $r^2 = x^2 + y^2$  and  $A \equiv \frac{Y}{4\pi}$ , where  $Y = 4\mu(\mu + \lambda)/(2\mu + \lambda)$  is the two-dimensional Young's modulus. Note that the functional form of the spatial dependence, being determined by geometry, is the same as for plane stresses around dislocations in three-dimensional solids. However, the relationship between  $A$  and the elastic constants

is different from a three-dimensional isotropic solid [18]. For a dislocation with  $\vec{b} = \pm b\hat{y}$  one has to take  $x \rightarrow y$  and  $y \rightarrow -x$  on the right hand side of the above equations.

On a cylinder, a dislocation at  $(x_0, y_0) = (0, 0)$  must be duplicated at intervals of  $W$  in the  $y$  direction, to respect the boundary conditions. Therefore the stresses at a point  $(x, y)$  generated by a dislocation with  $\vec{b} = b\hat{x}$  at the origin are given by:

$$\sigma_{xx}^x = \sum_{k=-\infty}^{\infty} \frac{-Ab[y + kW][3x^2 + (y + kW)^2]}{[x^2 + (y + kW)^2]^2}, \quad (5)$$

$$\sigma_{yy}^x = \sum_{k=-\infty}^{\infty} \frac{Ab(y + kW)[x^2 - (y + kW)^2]}{[x^2 + (y + kW)^2]^2}, \quad (6)$$

and

$$\sigma_{xy}^x = \sum_{k=-\infty}^{\infty} \frac{Abx[x^2 - (y + kW)^2]}{[x^2 + (y + kW)^2]^2}. \quad (7)$$

The superscript on the stresses reminds us that these are the stresses created by a dislocation with  $\vec{b} = b\hat{x}$ . Similar sums represent the stress produced by an edge dislocation with  $\vec{b} = \pm b\hat{y}$ .

The force on another dislocation at  $(x, y)$  due to this stress will then be given by the Peach-Koehler force [4, 33, 34]:

$$F_i = b_k \sigma_{jk} \epsilon_{ijz}, \quad (8)$$

where  $\epsilon_{ijz}$  is the Levi-Civita tensor. Explicitly, we have for  $\vec{b} = b\hat{x}$ :

$$F_x = b\sigma_{xy}, \quad (9)$$

$$F_y = -b\sigma_{xx}. \quad (10)$$

while for  $\vec{b} = b\hat{y}$ :

$$F_x = b\sigma_{yy}, \quad (11)$$

$$F_y = -b\sigma_{xy}. \quad (12)$$



### Summing the series

The sums of Eqs. (5) through (7) can be evaluated using the Sommerfeld-Watson transformation [36]. To demonstrate this for the first sum, consider the function  $g(z) = \cot(\pi z)$ , which has only simple poles of residue unity which lie on the  $x$  axis at integer values. The sum of Eq. (2) can then be written as the complex contour integral:

$$\oint_C g(z)f(z)dz, \quad (13)$$

with:

$$f(z) = -Ab \frac{(y/W + z)[3(x/W)^2 + (y/W + z)^2]}{W[(x/W)^2 + (y/W + z)^2]}. \quad (14)$$

Since  $f(z) \sim 1/z$  at large distances from the origin, we can deform the contour so that it captures only the poles of  $f(z)$  (note that the integral on the circle at infinity vanishes even though the decay is only  $\sim 1/z$ , due to the  $\cot(\pi z)$  term). Upon rewriting the function  $f(z)$  as:

$$f(z) = -(Ab/W) \frac{(y/W + z)[3(x/W)^2 + (y/W + z)^2]}{(z + (y + ix)/W)^2(z + (y - ix)/W)^2}, \quad (15)$$

we see that it has two poles of order 2. Summing the residues gives:

$$\begin{aligned} \sigma_{xx}^x &= \oint_C g(z)f(z)dz = \\ &= \frac{iAb\pi^2 x}{2W^2} (\csc^2(\pi(y - ix)/W) - \csc^2(\pi(y + ix)/W)) \\ &- \frac{\pi Ab}{2W} (\cot(\pi(y + ix)/W) + \cot(\pi(y - ix)/W)). \quad (16) \end{aligned}$$

In a similar fashion one obtains the other components of the stress produced by a dislocation with  $\vec{b} = b\hat{x}$ :

$$\begin{aligned} \sigma_{yy}^x &= \\ &- \frac{iAb\pi^2 x}{2W^2} (\csc^2(\pi(y - ix)/W) - \csc^2(\pi(y + ix)/W)) \\ &- \frac{\pi Ab}{2W} (\cot(\pi(y + ix)/W) + \cot(\pi(y - ix)/W)), \quad (17) \end{aligned}$$

$$\sigma_{xy}^x = -\frac{Ab\pi^2 x}{2W^2} (\csc^2(\pi(y - ix)/W) + \csc^2(\pi(y + ix)/W)). \quad (18)$$

To find the components of the stress tensor due to a dislocation with  $\vec{b} = b\hat{y}$ , we use the previously mentioned

substitution  $x \rightarrow y$ ,  $y \rightarrow -x$ , which leads immediately to:

$$\sigma_{xx}^y = \sigma_{xy}^x, \quad (19)$$

$$\sigma_{xy}^y = \sigma_{yy}^x. \quad (20)$$

Application of the Somerfeld-Watson transformation to the remaining component of the stress tensor leads to:

$$\begin{aligned} \sigma_{yy}^y &= -\frac{Ab}{2W} \pi [-2\coth[\pi(x - iy)/W] - 2\coth[\pi(x + iy)/W] \\ &+ \pi \frac{x}{W} (\operatorname{csch}[\pi(x - iy)/W]^2 + \operatorname{csch}[\pi(x + iy)/W]^2)]. \quad (21) \end{aligned}$$

### Asymptotic forms

It is natural to consider various limits for the stresses. For distances small compared to the cylinder's radius, it can be checked that the previous expressions all reduce to the flat space results, as must be the case. However, for large separations along the  $x$  direction (i.e., the cylinder axis), the behavior is different. For a dislocation with  $\vec{b} = b\hat{x}$ , we find that for  $|x| \gg W = 2\pi R$ :

$$\sigma_{xx}^x \approx -4\pi^2 A b e^{-2\pi|x|/W} (|x|/W^2) \sin(2\pi y/W), \quad (22)$$

$$\sigma_{yy}^x \approx 4\pi^2 A b e^{-2\pi|x|/W} (|x|/W^2) \sin(2\pi y/W), \quad (23)$$

$$\sigma_{xy}^x \approx 4\pi^2 A b e^{-2\pi|x|/W} (|x|/W^2) \cos(2\pi y/W), \quad (24)$$

while for a dislocation with  $\vec{b} = b\hat{y}$ , we have:

$$\sigma_{xx}^y \approx 4\pi^2 A b e^{-2\pi|x|/W} (|x|/W^2) \cos(2\pi y/W), \quad (25)$$

$$\begin{aligned} \sigma_{yy}^y &\approx 2\pi A(b/W) \cdot \operatorname{Sgn}(x) \\ &- 4\pi^2 A b e^{-2\pi|x|/W} (|x|/W^2) \cos(2\pi y/W), \quad (26) \end{aligned}$$

$$\sigma_{xy}^y \approx 4\pi^2 A b e^{-2\pi|x|/W} (|x|/W^2) \sin(2\pi y/W), \quad (27)$$

where  $\operatorname{Sgn}(x) = x/|x|$ . Thus, all components of the stress tensor decay exponentially, except for the circumferential stress induced by a dislocation with  $\vec{b} = b\hat{y}$ , which approaches to a constant value exponentially fast. This constant reflects the half-line of extra material that is inserted throughout the long axis of the cylinder, leading to a long-ranged stress field, as evident in the first term of Eq. (26).

### Energy considerations

In this section we convert our results for the stresses to the elastic interaction energies for two dislocations on a cylinder, obtained by integrating the Peach-Koehler force of Eq. (8). As discussed above, a generic Burgers vector can be decomposed into  $\hat{x}$  and  $\hat{y}$  components, and thus we consider three distinct scenarios:

(a) Both dislocations have Burgers vectors in the  $\pm\hat{x}$  directions.

(b) One dislocation with  $\vec{b} = \pm b\hat{x}$  with another with  $\vec{b} = \pm b\hat{y}$ .

(c) Both dislocations have Burgers vectors in the  $\pm\hat{y}$  directions.

In flat space, the interaction energy of two edge dislocations with vectors  $\vec{b}_1$  and  $\vec{b}_2$ , and with a relative separation of  $\vec{r} = (x, y)$ ,  $r \gg b$ , is given by [5]:

$$E(x, y) = -A \left( (\vec{b}_1 \cdot \vec{b}_2) \log\left[\frac{r}{b}\right] - \frac{(\vec{b}_1 \cdot \vec{r})(\vec{b}_2 \cdot \vec{r})}{r^2} \right) + 2E_c, \quad (28)$$

where  $b$  is the lattice spacing, and the effect of higher order terms in the gradient expansion of Eq. (1) is given by the core energy term  $2E_c$  [37]. Note that unless the Burgers vectors are equal and opposite, the total energy of the system will also include terms that diverge with the system size, as previously discussed.

The derivatives of the interaction energy with respect to the coordinates yield the forces: for example, differentiating Eq. (28) with respect to  $x$  or  $y$  and using Eqs. (9) and (10) gives Eqs. (4) and (2). Up to a constant, we can obtain this interaction energy by integration of the Peach-Koehler force.

Upon generalizing to the case of the cylinder, where we have already found an explicit formula for the forces, we can use it to derive the expression for the interaction energy for case (a) above. Integrating the force in the  $x$  direction,  $F_x = -b\sigma_{xy}^x$ , with respect to  $x$  leads to  $E(x, y) = Y(y) + C(x, y)$  with:

$$C(x, y) = \frac{Ab^2}{2} \log[\sinh(\pi(x - iy)/W)] + \frac{Ab^2}{2} i\pi(x/W) \csc(\pi y/W) \sinh(\pi x/W) \operatorname{csch}(\pi(x - iy)/W) + C.C., \quad (29)$$

with  $W = 2\pi R$ . The derivative of  $C(x, y)$  with respect to  $y$  can be shown to be equal to  $F_y = b\sigma_{xx}^x$ , implying that  $Y(y) = \text{const}$ . The constant can be found by demanding that the expression reduces to that of flat space for  $W \gg x, y$ , see Eq. (28). Our final result for antiparallel Burgers vectors along the cylinder axis is thus:

$$E_{\hat{x}, -\hat{x}}(x, y) = \frac{Ab^2}{2} \log\left[\frac{W}{\pi b} \sinh(\pi(x - iy)/W)\right] + \frac{Ab^2}{2} i\pi(x/W) \csc(\pi y/W) \sinh(\pi x/W) \operatorname{csch}(\pi(x - iy)/W) + C.C. \quad (30)$$

We have suppressed, for simplicity, the large distance core energy contribution displayed in Eq. (28). The notation  $E_{\hat{x}, -\hat{x}}$  denotes that this is the interaction energy of two antiparallel dislocations with Burgers vectors in the  $\pm\hat{x}$  directions. For  $x \gg R$ , we find that:

$$E_{\hat{x}, -\hat{x}} \approx Ab^2 \log\left[\frac{W}{2\pi b}\right] - 2Ab^2 \frac{|x|}{W} e^{-2\pi|x|/W} \cos(2\pi y/W). \quad (31)$$

Fig. 5 shows the equal energy contours of this interaction energy. Close to the origin, a cut parallel to the  $\hat{x}$ -axis would give a graph with two minima, corresponding to the two dislocations with separation vector at a 45 degrees angle to the  $\hat{x}$ -axis – the double minima are expected, since close to the origin we are not sensitive to the finite radius of the cylinder, and this is indeed the stable configuration of two dislocations in flat space, when climb processes (motion perpendicular to the Burgers vector) are prohibited [38]. The double minima structure at a fixed offset  $y = W/10$  is shown in Fig. 6. However, at larger vertical separations the minima become shallower and shallower, until at a separation of  $W/4$  along the circumference, there is only a single maximum at  $x = 0$ . For fixed  $y$ , the minima obey  $\frac{\partial E_{\hat{x}, -\hat{x}}(x, y)}{\partial x} \propto \sigma_{xy}^x = 0$ . Upon equating Eq. (18) to zero, we find (aside from the solution  $x = 0$ ):

$$\tan(\pi y/W) = \pm \tanh(\pi x/W), \quad (32)$$

which indeed has a solution at nonzero  $x$  provided  $y < W/4$ .

Taking the  $y \rightarrow 0$  limit of Eq. (30) (which is ill-defined for  $y = 0$ ) leads to:

$$E_{\hat{x}, -\hat{x}}(x, y \rightarrow 0) = Ab^2 \left( \log\left[\frac{2R}{b} \sinh(\pi x/W)\right] - \frac{\pi x}{W} \coth(\pi x/W) \right). \quad (33)$$

This formula is equivalent to Eq. (2.1b) in Ref. [38], describing the interaction energy of two antiparallel grain boundaries in the infinite plane. The connection between these two systems will be elucidated in section .

In a similar fashion we can find the interaction energy for case (b) above, of an edge dislocation with  $\vec{b} = b\hat{x}$  with another with  $\vec{b} = b\hat{y}$ . The forces on the latter are given by  $F_x = \sigma_{yy}^x$ ,  $F_y = -\sigma_{xy}^x$ . By integrating the stresses we find:

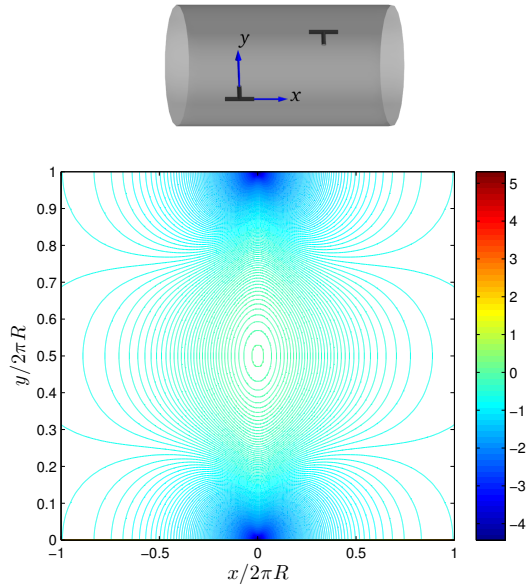


FIG. 5. Equipotential contours for a dislocation on a cylinder at position  $(x, y)$  with  $\vec{b} = -b\hat{x}$ , interacting with another dislocation at the origin with  $\vec{b} = b\hat{x}$ . Energy is measured in units of  $Ab^2$ . Note the much lower energies than in Fig. 8 where the Burgers vector are rotated by  $90^\circ$ .

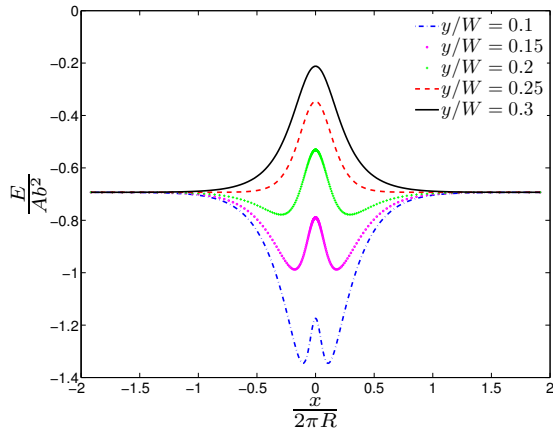


FIG. 6. Slice along the energy contours of Fig. 5 showing interaction energy as a function of  $x$ , for several ratios of  $y/W$ . Note the double minima, which become a single maximum for  $y \geq W/4$ .

$$E_{\hat{x},\hat{y}}(x, y) = -\frac{Ab^2\pi\frac{x}{W}\sin[2\pi y/W]}{\cos[2\pi y/W] - \cosh[2\pi x/W]}. \quad (34)$$

The equal energy contours of this interaction energy are shown in Fig. 7. For  $x \gg R$  the expression reduces to:

$$E_{\hat{x},\hat{y}} \approx 2\pi Ab^2 \frac{x}{W} \sin[2\pi y/W] e^{-2\pi|x|/W}.$$

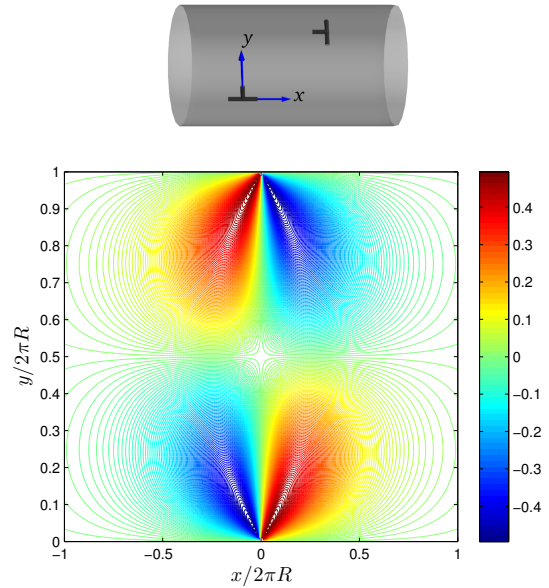


FIG. 7. Equipotential contours for a dislocation at  $(x, y)$  on a cylinder with  $\vec{b} = b\hat{y}$ , interacting with another dislocation at the origin with  $\vec{b} = b\hat{x}$ . Energy is measured in units of  $Ab^2$ . Note that the large distance core energy contribution, analogous to that appearing in Eq. (28), is undefined without additional dislocations on the cylinder, since the sum of the Burgers vectors should vanish. Nevertheless, this expression is useful for charge-neutral dislocation configurations on a cylinder, whose interactions can be decomposed into pairwise interactions involving  $E_{\hat{x},-\hat{x}}$ ,  $E_{\hat{y},-\hat{y}}$  and  $E_{\hat{x},\hat{y}}$ ; see Eqs. (31),(36) and (34).

For  $y = 0$ , we find that  $E_{\hat{x},\hat{y}} = 0$ . For  $x, y \ll W$ , Eq. (34) reduces to the flat expression:

$$E_{\hat{x},\hat{y}} \approx \frac{Ab^2xy}{x^2 + y^2} = \frac{Ab^2}{\frac{x}{y} + \frac{y}{x}}. \quad (35)$$

Since  $|c + \frac{1}{c}| \geq 2$  for any value of  $c$ , there is clearly no divergence of the energy as the two dislocations come together, with a minimum energy of  $-\frac{Ab^2}{2}$  obtained for  $x = -y$ . The finiteness of the energy as the dislocations as  $(x, y) \rightarrow (0, 0)$  reflects the vanishing of the logarithmic divergence in Eq. (28) when  $\vec{b}_1$  and  $\vec{b}_2$  are perpendicular. As mentioned before, a dislocation configuration where the sum of Burgers vectors does not vanish leads to additional terms in the expression of the total energy diverging with the system size. The above equations only reflect the pairwise interaction terms.

Finally, in case (c), the force on an edge dislocation with  $\vec{b} = -b\hat{y}$  induced by another dislocation with  $\vec{b} = b\hat{y}$  is given by  $F_x = -\sigma_{yy}^y$ ,  $F_y = \sigma_{xy}^y$ . Upon integration we

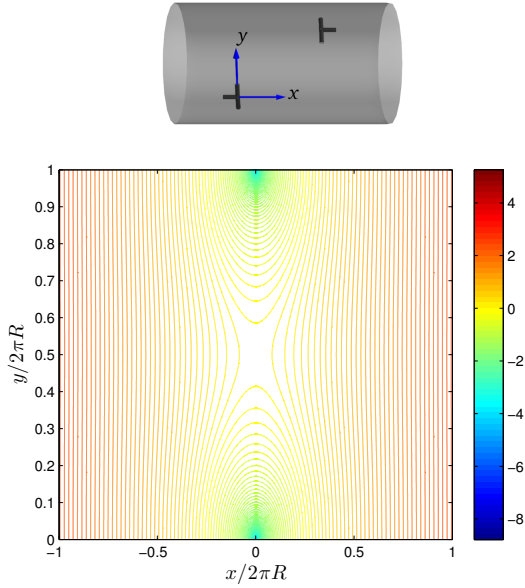


FIG. 8. Equipotential contours for a dislocation at  $(x, y)$  on a cylinder with  $\vec{b} = -b\hat{y}$ , interacting with another dislocation at the origin with  $\vec{b} = b\hat{y}$ . Energy is measured in units of  $Ab^2$ . Note that for  $x \gg R = W/2\pi$  the energy contours become parallel to the  $y$  axis; so that the forces are primarily in the  $x$  direction. This trend, and the associated linear potential, can be seen from Eqs. (11), (12),(26) and (27).

find

$$E_{\hat{y}, -\hat{y}}(x, y) = \frac{Ab^2}{2} \log\left[\frac{W}{e\pi b} \sinh[\pi(x - iy)/W]\right] - \frac{Ab^2}{2} i\pi(x/W) \csc[\pi y/W] \sinh[\pi x/W] \operatorname{csch}[\pi(x - iy)/W] + C.C., \quad (36)$$

where  $e$  is the base of the natural logarithm. The equal energy contours are shown in Fig. 8. The analytic form of Eq. (36) is similar (but not identical!) to that for  $E_{\hat{x}, -\hat{x}}$ , see Eq. (30). As before, we can check that for  $x, y \ll R$  this reduces to Eq. (28) (this correspondence requires the extra factor  $2/e$  in the logarithm). For  $x \gg R$  we now find, in contrast to Eq. (31), a linear potential,

$$E_{\hat{y}, -\hat{y}}(x, y) \approx \frac{2\pi Ab^2}{W} |x|. \quad (37)$$

In the limit  $y \rightarrow 0$ , similarly to the case of  $E_{\hat{x}, -\hat{x}}(x, 0)$ , we find that:

$$E_{\hat{y}, -\hat{y}}(x, 0) = Ab^2 \left( \log\left[\frac{W}{e\pi b} \sinh(\pi x/W)\right] + \frac{\pi x}{W} \coth(\pi x/W) \right) \quad (38)$$

### Stresses and energetics for Burgers vectors at arbitrary inclination angle

A Burgers vector  $\vec{b}$  that makes an angle  $\theta$  with the  $x$  axis, can always be decomposed into Cartesian components parallel and perpendicular to the cylinder axis. Since we assume *linear* elasticity, the relevant stress fields follow from the superposition of the solutions obtained previously:

$$\sigma_{ij}^\theta = \sigma_{ij}^x \cos \theta + \sigma_{ij}^y \sin \theta, \quad (39)$$

where  $\sigma_{ij}^x$  and  $\sigma_{ij}^y$  appear in Eqs. (16–21).

We now determine the interaction energy of this dislocation with another dislocation, whose Burgers vector forms an angle  $\alpha$  with the  $x$  axis (on a triangular lattice, if the Burgers vectors have their minimum allowed lengths, the difference of the two angles  $\theta$  and  $\alpha$  will be a multiple of  $\pi/3$ ). The force on this dislocation is then:

$$F_x = b[\sigma_{xy}^x \cos \theta \cos \alpha + \sigma_{xy}^y \sin \theta \cos \alpha + \sigma_{yy}^x \cos \theta \sin \alpha + \sigma_{yy}^y \sin \theta \sin \alpha]. \quad (40)$$

$$F_y = b[-\sigma_{xx}^x \cos \theta \cos \alpha - \sigma_{xx}^y \sin \theta \cos \alpha - \sigma_{xy}^x \cos \theta \sin \alpha + \sigma_{xy}^y \sin \theta \sin \alpha]. \quad (41)$$

Upon integration we find that:

$$E_{\theta, \alpha} = E_{x,x} \cos \theta \cos \alpha + E_{y,x} \sin(\theta + \alpha) + E_{y,y} \sin \theta \sin \alpha. \quad (42)$$

For the phyllotaxis problem discussed in section , the energy landscape associated with dislocation pairs with antiparallel Burgers vectors is of particular interest; these can nucleate locally and then unbind, thus modifying the geometry of the lattice. Fig. 9 shows an example of the energy equipotential contours for  $\theta = \pi/6$  and  $\alpha = 7\pi/6$ .

### Structure of the energy landscape

In this section we describe in more detail the structure of the interaction energy landscape for two dislocations interacting on the surface of a cylinder at zero temperature.

*Burgers vectors are in the  $\pm x$  directions*

In the case of dislocations with antiparallel Burgers vectors in the  $\pm \hat{x}$  directions, the interaction energy is given by Eq. (30). From the energy contours (see Fig. 5), we can see that the configuration where the two dislocations are located at the same  $x$  coordinate but on

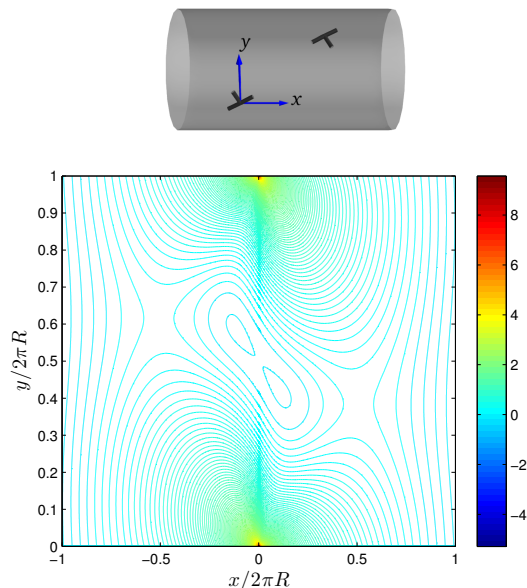


FIG. 9. Equipotential contours for a dislocation on a cylinder with a Burgers vector  $\vec{b} = b(\frac{\sqrt{3}}{2}\hat{x} + \frac{1}{2}\hat{y})$ , forming an angle of  $\pi/6$  with respect to the  $\hat{x}$ -axis, interacting with another dislocation with an opposite Burgers vector. The interaction energy is given by Eq. (42). Note the two skewed saddle points. Energy is measured in units of  $Ab^2$ .

opposite sides of the cylinder, the anti-podal point, is a maximum of the energy. If the two dislocations have the same sign, there is a stable minimum riding on top of an infinite energy due to the lack of overall charge neutrality. To see this, one can expand the force on a dislocation offset slightly from the origin by an amount  $(x, y)$ , exerted by another dislocation at the anti-podal point. This gives, for antiparallel Burgers vectors, to lowest non-vanishing order:

$$\begin{aligned} F_x(x, y) &= Kx, \\ F_y(x, y) &= Ky, \end{aligned} \quad (43)$$

with  $K = \frac{4\pi^2 b^2}{W^2} > 0$ , so the minimum is unstable. For parallel Burgers vectors, the signs are reversed.

We conclude that two dislocations with antiparallel Burgers vectors on opposite sides of the cylinder can minimize their energy by annihilating, while two dislocations of the same sign will remain at the anti-podal point to minimize the repulsive elastic interaction energy.

*Burgers vectors are in the  $\hat{x}$  and  $\hat{y}$  directions*

In this case the anti-podal point is found to be a saddle point, as can be seen near the center of Fig. 7. As before, we suppress an infinite energy due to the lack of charge neutrality.

*Burgers vectors are in the  $\pm y$  directions*

Upon repeating the same analysis for two dislocations with Burgers vectors in the  $\pm y$  directions, we find that, again, the only extremum point is at the anti-podal point  $(0, W/2)$ , which Fig. 8 shows to be a saddle point.

### NUMERICAL TEST ON A TRIANGULAR LATTICE

As discussed in the Introduction, in soft matter physics a triangular lattice of colloidal particles wrapped around a cylinder may be realizable. If one of the principal axes of the lattice is oriented along the circumferential direction, the minimal Burgers vector of a dislocation can take on the following values:  $\vec{b} = \pm b\hat{y}$ ,  $\vec{b} = \pm b\left(\frac{\sqrt{3}}{2}\hat{x} \pm \frac{1}{2}\hat{y}\right)$ .

To test our continuum limit predictions numerically, consider the stresses associated with an isolated dislocation at the origin with Burgers vector  $\vec{b} = b(\frac{\sqrt{3}}{2}\hat{x} - \frac{1}{2}\hat{y})$  (i.e.  $\theta = -\pi/6$ ) in a triangular lattice of masses and harmonic springs which are relaxed to their minimum energy configuration by a conjugate gradient method. To insure a charge-neutral configuration, an additional dislocation with antiparallel Burgers vector was created at the negative  $\hat{x}$  end of the cylinder. The strains and stresses at any point can be calculated from the shift in position of the surrounding points relative to the perfect lattice. In Fig. (10), we display  $\sigma_{xx}$  and  $\sigma_{yy}$  for positive  $x$  at a constant  $y = W/4$  for cylinders of various sizes. We obtain good agreement with our continuum results even for relatively small system sizes, which can be realized in colloidal experiments. This calculation illustrates the applicability of our results for Burgers vectors rotated away from the  $x$ -axis, which lead to long range strain fields along the cylinder axis.

We note from Fig. (10) that the asymptotic value of  $\sigma_{yy}$  at large positive  $x$  in the simulations is zero rather than  $\sigma_{yy}^{-\pi/6}(x \rightarrow \infty) = -\pi A/W$  predicted from Eq. (39). This is due to the contribution of the additional dislocation positioned at the negative  $\hat{x}$  end of the cylinder: from Eqs. (23), (22), (24) we see that while it has an exponentially small effect on the other components of the stress tensor, it creates a *constant* circumferential stress  $\sigma_{yy}$ , thus shifting the values for the circumferential stress by a constant. At  $x \gg W$ , the stress created by the dislocation at the origin is also approximately constant, and since the two dislocations are antiparallel their contributions are equal but of opposite sign – which explains why  $\sigma_{yy} = \sigma_{yy}^{-\pi/6} + \sigma_{yy}^{5\pi/6} \rightarrow 0$  at large positive  $x$ .

There is some evidence for helical motion of tracer particles on the cell walls of elongating bacteria such as *Escherichia coli* [39], suggesting that the lattice shown in Fig. 3 may be slightly skewed. Hence, it is of some interest to find the asymptotic form as  $x \rightarrow \infty$  of the stress for



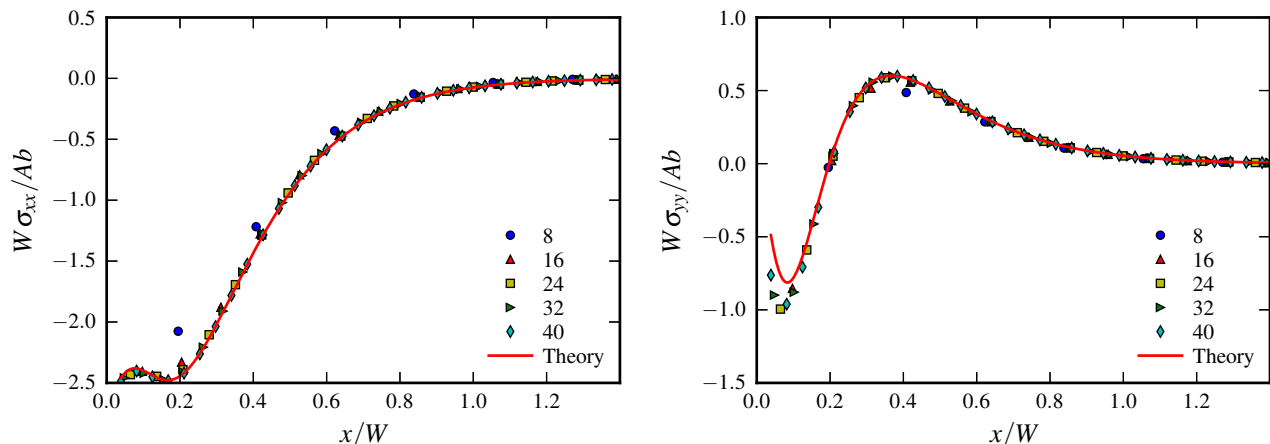


FIG. 10. Stress components  $\sigma_{xx}$  (left) and  $\sigma_{yy}$  (right) as a function of  $x$  at a constant offset around the cylinder  $y = W/4$ , for a dislocation with  $\vec{b} = b(\frac{\sqrt{3}}{2}\hat{x} - \frac{1}{2}\hat{y})$  at the origin. To account for a charge-neutral dislocation configuration, another dislocation with an antiparallel Burgers vector is placed along the negative  $\hat{x}$  end of the cylinder, far enough from the origin to create a constant  $\sigma_{yy}$  stress [see Eq. (26)] and a negligible contribution to the other components of the stress tensor. The symbols are for simulations of cylinders with  $W$  increasing from  $8b$  to  $40b$  where  $b$  is the equilibrium lattice constant of the simulation lattice. In all cases, the length of the cylinder is  $8.66W$  and the dislocation is situated at the center of the cylinder along the long axis to minimize edge effects. The solid line is the theoretical prediction from Eq. (39) with  $\theta = -\pi/6$ , where for the right figure one has to add the constant  $\sigma_{yy}$  stress mentioned above. Except for one or two points closest to the dislocation, where discrete effects become important, the simulations agree with the results of continuum elasticity even for relatively small system sizes ( $W \gtrsim 16b$ ). For negative values of  $x$ , the convergence to the continuum limit results is slower, and there are corrections to the stresses which scale as  $\sim b/W$ . These will be discussed in more detail in future work.

a dislocation with a Burgers vector in a direction forming a small angle  $\theta$  with the  $\hat{x}$  axis. We use Eqs. (26) and (39) to find:

$$\begin{aligned} \sigma_{yy} &\approx \theta \cdot 2\pi Ab/W \cdot Sg(x) \\ &+ 4\pi^2 Abe^{-2\pi|x|/W} |x|/W^2 [\sin(2\pi y/W) - \theta \cos(2\pi y/W)]. \end{aligned} \quad (44)$$

Thus, for slightly tilted Burgers vectors there is a length scale  $l^*$  along  $\hat{x}$  at which the constant contribution to the stress dominates over the exponentially decaying one, which is readily found by equating the two terms:

$$[2\pi e^{-2\pi l^*/W} l^*/W] \sin(2\pi y/W) = \theta. \quad (45)$$

Provided  $y$  is not too small, with  $W = 2\pi R$ , we find that to leading order:

$$l^* \sim R \log(\theta). \quad (46)$$

## ANALOGY WITH GRAIN BOUNDARIES

We now describe a correspondence between dislocations on a cylinder and grain boundaries, which allows checks of some of our calculations [40].

Suppose that the lattice orientation on the cylinder allows two dislocations of opposite Burgers vectors,  $\pm b\hat{x}$ , initially very close together. Let us now glide one of the dislocations away from the other, until they reach a certain separation  $\Delta$  along the  $\hat{x}$ , which coincides with the axis of cylindrical symmetry. Every time the dislocation glides by one lattice spacing, we connect an initially circumferential row with an adjacent one to make a spiral. Thus, at any fixed separation, the finite part of the cylinder between the two dislocations is converted to a *helical* structure, which can be thought of as a local rotation of the crystalline lattice (see Fig. 4). Since a shift of  $b$  is associated with each rotation, the pitch of the helix is  $\theta = b/W$ . Therefore, we can view the circumferential row passing through each of the dislocations as a *grain boundary*, and the whole structure as a polycrystalline material with three regions, the middle one tilted by  $\theta$ . Glide separation and the equivalent grain boundary configuration are also illustrated in Fig. 11, as well as in the Supplementary Video S1, showing numerical results for a system of masses and springs, where the minimal energy configuration of the system at each instance in time is obtained by a conjugate gradient minimization procedure.

By this analogy, the interaction energy  $E(x, y)$  of two dislocations on the cylinder separated by a displacement  $(x, y)$ , corresponds to the energy (per section of length  $W$ ) of two infinite, straight, grain boundaries a distance

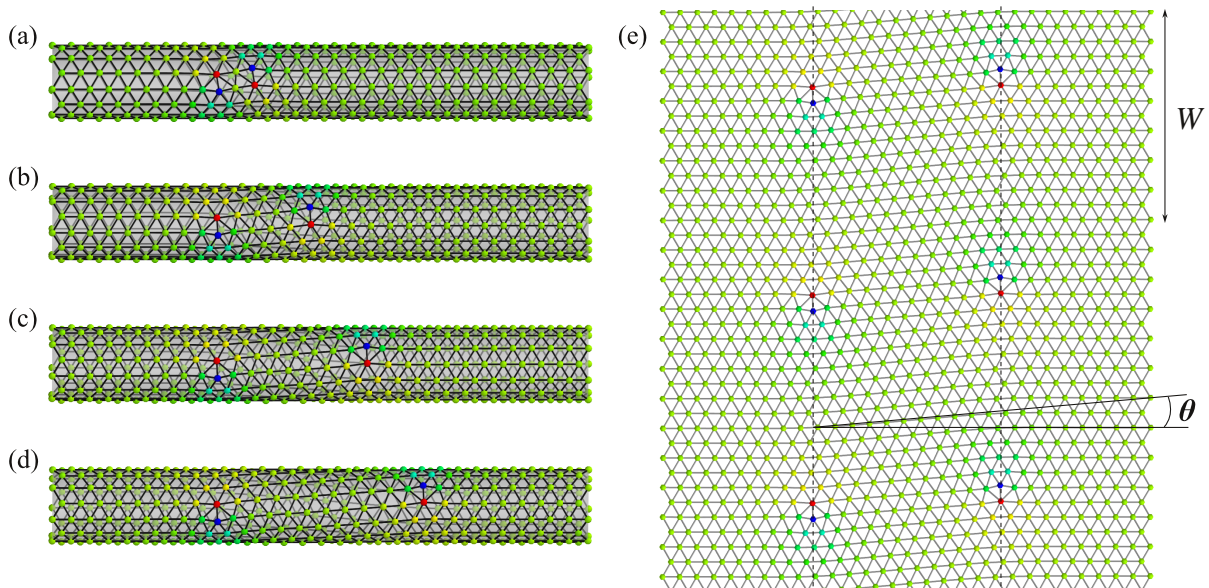


FIG. 11. Dislocations on a cylinder are analogous to grain boundaries. The images show configurations obtained numerically for a hexagonal lattice of masses and harmonic springs whose energy is minimized as the dislocation pair is separated by a glide. On this triangular lattice, a dislocation corresponds to a point with five neighbors adjacent to a point with seven neighbors. Starting with two nearby dislocations, (a), we glide one of the dislocations to the right in steps of the lattice spacing [Supplementary Video S1; figures (b–d) show intermediate snapshots during the glide]. The finite section of the cylinder between the two dislocations displays a helical structure, similar to the model with magnetic beads shown in Fig. 4. The analogy with a *flat* polycrystalline material is illustrated by unrolling the cylindrical crystal in (d) and duplicating it several times in the  $y$  (circumferential) direction to replicate the periodic boundary conditions (e). The resulting infinite columns of dislocations (dotted lines) define two grain boundaries separating the middle region, rotated by an angle  $\theta = b/W$ , from sections with the original crystal orientation on either side.

$x$  apart and offset by an amount  $y$  along their lengths, where the distance between adjacent dislocations in each grain boundary is  $W$ . As is well known in the theory of small angle grain boundaries [4, 38], the associated grain boundary angle is  $\theta = b/W$ . For example, the interaction energy of two parallel grain boundaries with Burgers vectors in the  $\pm\hat{x}$  directions and separated by a distance  $x$ , mathematically equivalent to the situation in Fig. 11(e), is given by Eq. (33); This is in agreement with Eq. (2.1b) in Ref. [38].

### ENERGY LANDSCAPE IN THE PRESENCE OF A CONSTANT AZIMUTHAL FORCE

Consider two dislocations with antiparallel Burgers vectors  $\pm b\hat{x}$  on a cylinder, a small distance apart. For simplicity, we pin one dislocation at the origin. Let us assume that there is an additional constant force acting on it, due, say, to the Peach-Koehler force created by an external stress  $\sigma_{xx}$  [see Eq. (10)].

The energy landscape now resembles a tilted washboard potential with period  $W$  and is given by:

$$E_{\hat{x},-\hat{x}}^F(x,y) = \frac{Ab^2}{2} \log\left[\frac{W}{\pi b} \sinh(\pi(x-iy)/W)\right] + \frac{Ab^2}{2} i\pi(x/W) \csc(\pi y/W) \sinh(\pi x/W) \operatorname{csch}(\pi(x-iy)/W) + C.C. - Gy, \quad (47)$$

where the constant azimuthal force  $G \propto \sigma_{xx}$ . For climb dynamics, there can also be a contribution due to the chemical potential associated with adding new material [9]. The dynamics of the dislocation pair in this potential will depend on the glide and climb mobilities to be introduced below. First, however, we discuss how the energy landscape changes due to the field  $G$ . Clearly, the minimum at the origin remains if the field  $G$  is not too large. Now, however, there are important new *saddle points* in the energy landscape. Let us first locate these saddles in the case of flat space. Here, the potential is given by Eq.

(28), with an additional term  $-Gy$ . A necessary condition for the existence of a saddle is the vanishing of  $\frac{\partial E}{\partial x}$  and  $\frac{\partial E}{\partial y}$ . Upon differentiation of  $E_{\hat{x},-\hat{x}}^F(x,y)$  we obtain:

$$x_{saddle} = y_{saddle} = \frac{Ab^2}{G}. \quad (48)$$

This extremum must be a saddle point since (a) for a given  $y$  coordinate there is a minimum energy at  $x = y$  [see discussion preceding Eq. (32)], and (b) this cannot be a minimum in the  $y$  direction since  $y \rightarrow 0$  and  $y \rightarrow \infty$  give us a negative, diverging energy.

Let us now consider the problem on a cylinder. The only scales that may enter the problem are  $Ab^2$ ,  $W$  and  $G$ ;  $b$  cannot enter explicitly since we are considering the continuum limit. Only one dimensionless parameter can be formed out of these, namely:  $D \equiv GW/Ab^2$ . Therefore the  $y$  position of the saddle (which as we show below exists for any value of  $G$ ), can be written as:

$$y_{saddle} = \frac{Ab^2}{G} f(D), \quad (49)$$

where  $f(D)$  is a function of the dimensionless parameter  $D$ . The case of flat space, Eq. (48), corresponds to  $D \rightarrow \infty$ , showing that  $f(D)$  must asymptotically approach the value one. We now proceed to discuss the general form of  $f(D)$ . The condition  $\frac{\partial E}{\partial x}$  does not depend on the field in the  $y$  direction, and thus, Eq. (32) still holds. Therefore, we search for the saddles whose coordinates have the form  $(x^*(y), y)$ , where:

$$x^*(y) = \pm \frac{W}{\pi} \operatorname{arctanh}(\tan(\pi y/W)), \quad (50)$$

with  $0 < y < W/4$ .

Within this parametrization, we still have to satisfy  $\frac{\partial E}{\partial y} = 0$ . This condition implies that  $F_y = G - b\sigma_{xx}^x = 0$ , with  $\sigma_{xx}^x$  given by Eq. (16). For small values of  $y$ , a vanishing derivative in the  $x$  direction would yield  $x^*(y) = y$ , as can also be seen from Eq. (50). For such a point, we know that the two dislocations have a large force in the  $y$  direction pulling them together, which can be seen directly from Eq. (2) (since in this regime we are not sensitive to the cylindrical geometry). On the other hand, for  $y$  very close to  $W/4$ , Eq. (50) yields an  $x$  coordinate which diverges. Hence, the stress in Eq. (16) must vanish, since the force between two dislocations falls off as a power-law. This argument implies that the  $y$  component of the force at such a point will be approximately  $G$ , and in particular, it will be *positive*. Therefore, there is an intermediate value of  $y$  for which both  $F_x$  and  $F_y$  vanish. We conclude that a saddle exists for any value of  $G$ ! (In fact, two saddles, since we have a reflection symmetry around the  $y$  axis.) Equipotential contours where the saddles can be seen are shown in Figs. (12) and (13),

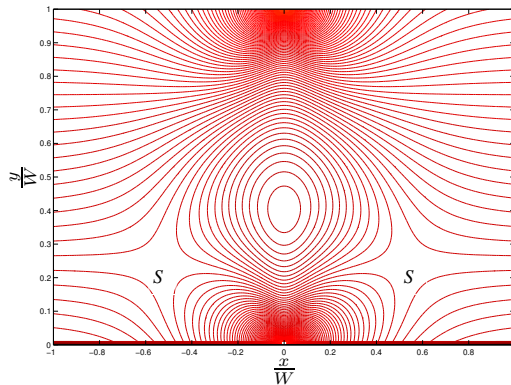


FIG. 12. Equipotential contours for a dislocation pair with  $\frac{GW}{Ab^2} = 1$ , with  $W = 2\pi R$ . Note that the force  $G$  caused by a macroscopic stress  $\sigma_{xx}$  has pulled the maximum away from  $y = W/2$ . Note also the two saddle points (denoted by the letter  $S$ ) near  $y \approx W/4$ .

for values  $\frac{GW}{Ab^2} = 1$  and a much stronger force given by  $\frac{GW}{Ab^2} = 10$ , respectively. For large values of  $G$ , the saddles coincide with those obtained for flat space. However, for small  $G$  the saddles will be close to the line  $y = W/4$  and their  $x$  values will *diverge*. Fig. (14) shows this scaling, expressed in Eq. (49), and the asymptotic limits: for  $GW/Ab^2 \rightarrow \infty$ , the rescaled  $y$  coordinate of the saddle  $\frac{yG}{Ab^2}$  approaches unity, corresponding to the flat space result. For the opposite case,  $\frac{yG}{Ab^2} \approx \frac{WG}{4Ab^2}$ , corresponding to the straight line  $f(D) = D/4$ . To determine the form of the divergence of the  $x$  position of the saddle for small  $G$ , note from Eq. (22) that at large values of  $x$  the force in the  $y$  direction decays exponentially for any value of  $y$ , as:

$$F_y \approx [4\pi^2 Ab^2 e^{-2\pi x/W} x/W^2] \sin(2\pi y/W). \quad (51)$$

Upon equating this force to  $G$ , we find for small  $G$  a saddle at  $x^* \sim -\frac{W}{2\pi} \log\left(\frac{GW}{Ab^2 4\pi \log(GW/Ab^2)}\right)$ , a location that diverges approximately logarithmically as  $G \rightarrow 0$ .

An important feature of the saddle when considering the thermal excitation of dislocation pairs is its energy relative to, say, the interaction energy of the two dislocations when they are one lattice spacing apart. This energy difference is plotted in Fig. 15. For flat space, it is easy to see that the energy barrier diverges logarithmically as  $G \rightarrow 0$ , and is given by:

$$U(G) \approx Ab^2 \log(Ab/G), \quad (52)$$

where the energy is measured relative to that of a dislocation pair separated by a lattice constant  $b$ .

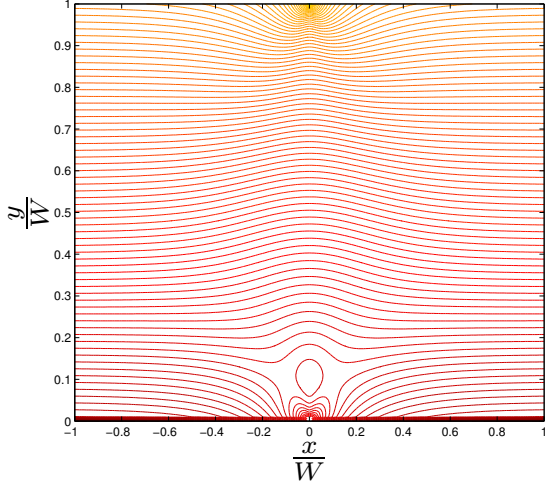


FIG. 13. Equipotential contours for a dislocation pair with  $\frac{GW}{Ab^2} = 10$ . Note the maximum and two saddle points near the line  $y = W/10$ .

Eq. (52) is approximately correct on the cylinder as well, provided the  $y$  coordinate of the saddle is much less than  $W$ . For small values of  $G$ , more careful analysis is required. Let us parametrize the saddle point by  $(x^*(y), y)$ . From Eq. (18) we infer that at large values of  $x$  the force in the  $x$  direction decays exponentially for any value of  $y$ , as:

$$F_x \approx [4\pi^2 Ab^2 e^{-2\pi x/W} x/W^2] \cos(2\pi y/W). \quad (53)$$

Hence, the potential at infinity does not diverge, leading to a finite energy barrier for dislocation unbinding at any value of  $G$ , as shown in Fig. (15). We can adapt the scaling analysis for the  $y$  coordinate of the saddle also to the energy. Consider the interaction energy  $E(x, y)$  in the absence of  $G$ . Although the lattice spacing  $b$  enters the expression for the interaction energy explicitly, it can be easily eliminated: from Eq. (31) we see that

$$E(x, y) = Ab^2 \log(W/b) + Ab^2 h[x/W, y/W], \quad (54)$$

which can also be deduced from dimensional considerations combined with the flat space limit. The energy  $U(G)$  is thus given by:

$$U(G) = E(x_{saddle}, y_{saddle}) - E(|\vec{r}| = b) - Gx_{saddle}. \quad (55)$$

Previously we found that the  $y$  coordinate of the saddle point scales as  $y_{saddle} = \frac{Ab^2}{G} f(D)$ , see Eq. (49). The same argument can be repeated for the  $x$  coordinate of the saddle, giving  $x_{saddle} = \frac{Ab^2}{G} g(D)$ , where the function  $g$  also depends on the dimensionless parameter  $D$ . Plugging these results into Eq. (55) and using Eq. (54) we find that:

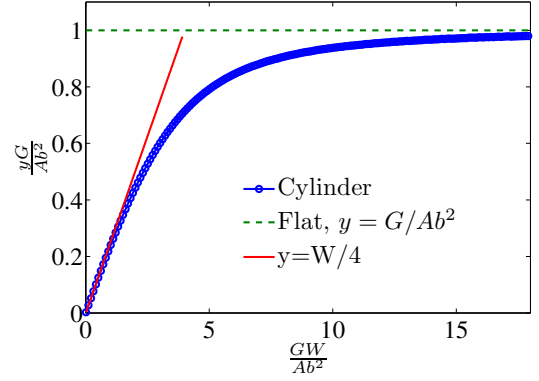


FIG. 14. The rescaled  $y$  coordinate of the saddle point  $\frac{yG}{Ab^2}$  is shown as a function of the dimensionless parameter  $\frac{GW}{Ab^2}$ . The horizontal line is the result in flat space, where  $y = \frac{Ab^2}{G}$ .

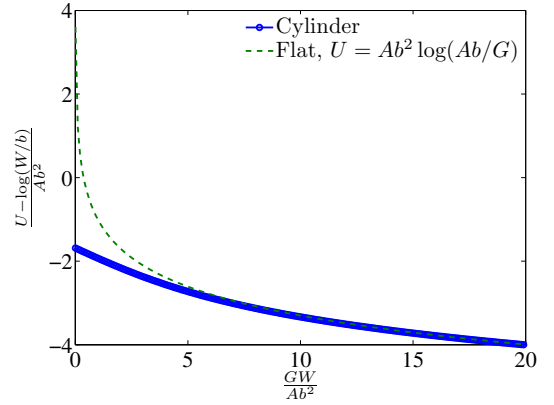


FIG. 15. The saddle point excitation energy  $U$ , given by Eq. (31), is rescaled and plotted as a function of  $\frac{GW}{Ab^2}$ . In the flat space limit the scaling function is given by  $\eta(D) = -\log(D)$ , corresponding to  $U = Ab^2 \log(Ab/G)$ . For the opposite case, when  $G$  is small and the cylindrical geometry is important, the energy  $U$  saturates at a constant value even as  $G \rightarrow 0$ ,  $\frac{U}{Ab^2} \approx const + \log(\frac{W}{b})$ .

$$U(G) = Ab^2 \eta(D) - Ab^2 \log(b/W), \quad (56)$$

with  $\eta(D) = h[\frac{g(D)}{D}, \frac{f(D)}{D}] - g(D)$  a function of the dimensionless parameter  $D$ . Rearranging the above equation, we find a dimensionless scaling form:

$$\frac{U(G) - Ab^2 \log(W/b)}{Ab^2} = \eta(D), \quad (57)$$

For flat space, we have  $U(g) = Ab^2 \log(Ab/G)$ , showing that for large values  $\eta(D) \approx -\log(D)$ . The above form of scaling is illustrated in Fig. 15.

**THERMAL NUCLEATION OF DISLOCATION  
PAIRS: A TWO-DIMENSIONAL ESCAPE OVER  
A BARRIER PROBLEM**

With colloidal particle arrays or bacterial cell walls at relatively high temperatures in mind, we shall now calculate the thermal nucleation rate of dislocations: in the presence of a uniform external field denoted  $G$ , two dislocations of opposite Burgers vectors can overcome the energy barrier due to their attractive interaction and unbind due to thermal fluctuations. We shall first treat this process in flat space, and then compare to the results in cylindrical geometry, which differ significantly when  $G$  is small. Our analysis will be done for the case of dislocations with Burgers vectors  $\pm b\hat{x}$ , where the external force driving the nucleation is in the  $\hat{y}$  direction, perpendicular to the Burgers vectors. For simplicity, we assume isotropic elastic constants. The same strategy can be adapted to other scenarios. We then discuss the nucleation of dislocations along the cylinder axis due to a *twisting* stress  $\sigma_{xy}$ .

**Nucleation of dislocations in flat space**

We consider first the thermal escape-over-a-barrier problem for two dislocations in flat space (similar results should hold for a cylinder with a large enough field  $G$  such that the saddle distance from the origin is much smaller than  $W$ ). It is convenient to assume that one of the dislocations is mobile, while the other is pinned at the origin. Alternatively, we can consider the motion relative to the fixed center-of-mass of the dislocation pair. For a similar analysis of thermal activation of vortex pairs in superfluid helium films, see Ref. [41]. Throughout this section, we choose units such that the Boltzmann constant  $k_B = 1$ .

We shall assume over-damped dynamics for the mobile dislocation, described by an anisotropic diffusion tensor  $\mathbf{D}$  [42]. We analyze the scenario where the dislocations can *glide* and *climb*. This choice is motivated by the bacterial elongation problem discussed in section , where it is the climb of dislocations that drives the growth process. The motion of dislocations for colloidal arrays on a cylinder could also have a climb component, provided the particles can jump on and off the cylinder, thus providing an external source of vacancies and interstitials. Notice that allowing climb mobility is very different from the situation in Ref. [38], where dislocations can only glide and one has a one-dimensional escape-over-a-barrier problem, rather than the *two-dimensional* problem that we study here.

The probability  $n(\vec{r}, t)$  of finding the dislocations with separation  $\vec{r}$  is given by the continuity equation:

$$\frac{dn}{dt} + \text{div}\vec{j} = 0, \quad (58)$$

with a probability current  $\vec{j}(\vec{r}, t)$ :

$$\vec{j} = \mu n \vec{F}(\vec{r}) - \mathbf{D} \vec{\nabla} n. \quad (59)$$

The first term is given by  $\vec{F}(\vec{r}) = -\vec{\nabla}U(\vec{r})$ , where the potential energy  $U(\vec{r})$  is the sum of the interaction of the two dislocations as given by Eq. (31) and the potential  $-Gy$  associated with the external driving force. Sufficiently close to equilibrium, the Einstein relation relates the diffusion tensor to the mobility tensor:  $\mathbf{D} = T\mu$ , allowing us to recast the Fokker-Planck equation as (setting  $k_B = 1$ ):

$$\frac{dn}{dt} = -\vec{\nabla}[-\mathbf{D}e^{-U/T}\vec{\nabla}(ne^{U/T})]. \quad (60)$$

We now exploit Langer's formalism [12] to determine the structure of the probability currents that describe the nucleation of dislocation pairs.

For small enough escape rates (*i.e.*, a low enough temperature), the process will be dominated by currents flowing near the saddle points of the potential energy landscape. In the case of a dislocation pair in flat space there are two symmetric saddles; the total escape rate will be double the probability current flowing through one of them.

The escape rate through the saddle includes the Hessian (matrix of second derivatives) around it. We denote the Hessian in the vicinity of the saddle by  $\mathbf{H}_{\text{saddle}}$ , and the Hessian in the vicinity of the minimum by  $\mathbf{H}_{\text{min}}$  (for dislocation pairs, the latter requires a short distance cutoff of order the lattice spacing  $b$ ). The probability density around the minimum follows a Boltzmann distribution, since thermalization in that region is a fast process compared to the time scales associated with crossing the high barriers. It is useful to define the transition matrix  $\mathbf{A}$  as:

$$\mathbf{A} = \mathbf{D}\mathbf{H}_{\text{saddle}}, \quad (61)$$

and denote its two eigenvalues by  $\lambda_1 > 0$  and  $\lambda_2 < 0$ .

The escape rate  $\Gamma$  is then given by [13] :

$$\Gamma = \frac{\lambda_1}{2\pi} \sqrt{\frac{\det[\mathbf{H}_{\text{min}}]}{|\det[\mathbf{H}_{\text{saddle}}]|}} e^{-U_{\text{saddle}}/T}. \quad (62)$$

We shall assume that  $\mathbf{D}$  is anisotropic but is diagonal in a basis where one of the eigenvectors coincides with the direction of the Burgers vector, say,  $\hat{x}$ . In this basis:

$$\mathbf{D} = \begin{pmatrix} D_g & 0 \\ 0 & D_c \end{pmatrix}, \quad (63)$$



where  $D_c$  and  $D_g$  are the glide and climb diffusion coefficients. As mentioned before, for bacterial cell wall growth dislocation motion is predominantly via climb, *i.e.*,  $D_c \gg D_g$ . For the case of colloids on a cylinder, we would typically have glide dynamics, *i.e.*,  $D_g \gg D_c$ .

Upon finding the positions of the two symmetric saddle points and calculating their Hessians, we obtain:

$$\mathbf{H}_{\text{saddle}} = \frac{G^2}{2Ab^2} \begin{pmatrix} 1 & -1 \\ -1 & -1 \end{pmatrix} \quad (64)$$

It follows that  $\sqrt{|\det[\mathbf{H}_{\text{saddle}}]|} = \frac{G^2}{\sqrt{2}Ab^2}$ , and  $\lambda_1 = \frac{G^2}{Ab^2} [\frac{D_g - D_c}{2} + \frac{1}{2}\sqrt{(D_c - D_g)^2 + 8D_cD_g}]$ .

Eq. (62) then leads to an escape rate given by:

$$\Gamma \propto \left[ \frac{D_g - D_c}{2} + \frac{1}{2}\sqrt{(D_c - D_g)^2 + 8D_cD_g} \right] e^{-U_{\text{saddle}}/T}, \quad (65)$$

with  $U_{\text{saddle}} = Ab^2 \log(\frac{Ab^2\sqrt{2}}{G}) + C$ , according to Eq. (31), with  $C$  a constant depending on the non-universal details associated with  $\det[\mathbf{H}_{\text{min}}]$ .

The proportionality constant for the rate in Eq. (65) will depend on the details of the dislocation nucleation at the origin, which should be independent of  $G$ . We conclude that the escape rate goes to zero as a power-law as  $G \rightarrow 0$ :

$$\Gamma \propto \left( \frac{G}{Ab} \right)^{\frac{Ab}{T}}. \quad (66)$$

### Nucleation of dislocations on a cylinder

We now solve the escape problem on a cylinder. The result for flat space should hold for large enough  $G$  so that  $\frac{Ab^2}{G} \ll W$ . When this inequality is reversed, however, the saddles will occur (as discussed above) at a point with large  $x$  and  $y \approx W/4$ , with  $U_{\text{saddle}}$  approaching a finite, maximal value  $U_{\text{barrier}}$ , independent of  $G$  (see Fig. 15). Consider the form of  $\mathbf{H}_{\text{saddle}}$  in this regime. From Eqs. (24) and (22) we know the asymptotic form of  $\frac{\partial E}{\partial x}$  and  $\frac{\partial E}{\partial y}$  for large  $x$ . With this information we can calculate the Hessian,

$$\mathbf{H}_{\text{saddle}} = \frac{G^2}{Ab^2} \begin{pmatrix} -\frac{\partial F_x}{\partial x} & -\frac{\partial F_x}{\partial y} \\ -\frac{\partial F_y}{\partial x} & -\frac{\partial F_y}{\partial y} \end{pmatrix}. \quad (67)$$

A straightforward calculation yields:

$$\mathbf{H}_{\text{saddle}} = [8\pi^3 Ab^2 2\pi x / W^3 e^{-2\pi x / W}] \mathbf{M}(y), \quad (68)$$

where the matrix  $\mathbf{M}$  is given by the  $y$  coordinate of the saddle:

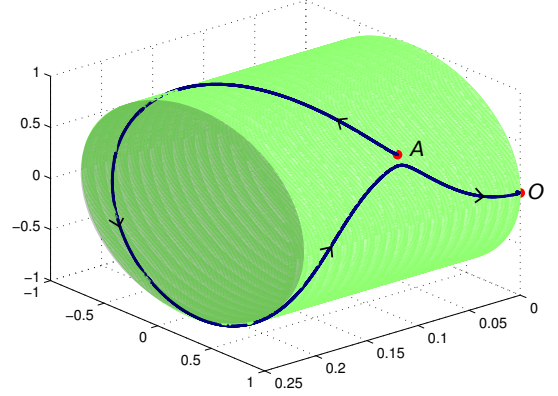


FIG. 16. A mobile dislocation, initially at point  $A$ , interacting with a pinned dislocation with antiparallel Burgers vector at the origin  $O$ . The first dislocation is placed just beyond the saddle point, at  $(x, y) = (\frac{W}{10}, \frac{W}{10})$ , for  $\frac{GW}{Ab^2} = 10$  (for a flat space, this would be the exact position of the saddle, however on a cylinder this point lies beyond it). The temperature is close to zero, although we assume motion over the Peierls potential [4] is possible. Here,  $W = 2\pi R = 1$ , and the isotropic mobility tensor components are  $\mu_c = \mu_g = 1$ . After completing one loop, the dislocation is “recaptured” and annihilates with the dislocation at the origin.

$$\mathbf{M} = \begin{pmatrix} \cos(2\pi y/W) & \sin(2\pi y/W) \\ \sin(2\pi y/W) & -\cos(2\pi y/W) \end{pmatrix}. \quad (69)$$

Since  $y \approx W/4$ , we have:

$$\mathbf{M} \approx \begin{pmatrix} 0 & 1 \\ 1 & 0 \end{pmatrix}, \quad (70)$$

Using Eq. (62) we therefore obtain that:

$$\Gamma \propto \sqrt{D_c D_g} e^{-E_{\text{barrier}}(G)/T}. \quad (71)$$

Thus, as the field  $G$  becomes weaker, and the cylindrical geometry becomes more important, the escape rate decreases but saturates at a finite value! Note, however, that the escape problem on a cylinder does not fit precisely to the conditions of the Kramers problem: one of the usual assumptions is that once the particle escapes, it can never be recaptured. Here, however, the opposite is true: the two dislocations can never truly escape from each other, due to the periodic boundary conditions. At low temperatures, the mobile dislocation is very likely to be “recaptured” and annihilated by its antiparallel partner after completing a single revolution, as depicted in Fig. 16. At finite temperatures, more revolutions are possible before recapture.

### Nucleation of gliding dislocations along the cylinder axis

Motivated by the bacterial elongation problem, in the previous example the dislocations had a finite *climb* mobility. For a crystal of colloids, however, the motion of dislocations is predominately via their *glide*, as previously mentioned. With this motivation in mind, we set  $D_c = 0$  in Eq. (63) and consider the unbinding of a pair of dislocation with  $\vec{b} = \pm\vec{x}$  on a triangular lattice, where an external  $\sigma_{xy}$  stress tensor causes the dislocations to glide away from each other. Note that in spite of the periodicity condition induced by the cylindrical geometry, this component of the stress tensor is *not* quantized, as explained in Appendix B.

The  $\sigma_{xy}$  stress creates a force along the  $\hat{x}$  axis, which is the glide direction. In this case, we have a *one-dimensional* escape-over-a-barrier problem, similar to that of Ref. [38], where the escape problem is solved in flat space. The potential in our case is different due to the cylindrical geometry, and is given by:

$$U(x) = \frac{Ab^2}{2} \log\left[\frac{2R}{b} \sinh(\pi(x-iy)/W)\right] + \frac{Ab^2}{2} i\pi(x/W) \csc(\pi y/W) \sinh(\pi x/W) \operatorname{csch}(\pi(x-iy)/W) + C.C - b\sigma_{xy}x, \quad (72)$$

similar to the nucleation problem discussed above with  $G = b\sigma_{xy}$ .

For large enough  $\sigma_{xy}$ , the maximum of the potential occurs for  $x = Ab/\sigma_{xy} \ll W$ , in which case the cylindrical geometry plays no role. Let us consider the opposite limit, namely,  $W\sigma_{xy} \ll Ab$ . In this case the maximum will occur for  $x_{max} \gg W$ , where the potential decays exponentially. In infinite flat space, the barrier for nucleation would diverge logarithmically as  $\sigma_{xy} \rightarrow 0$ , as discussed in Ref. [38]. Here, on the other hand, the interactions are bounded, and thus the nucleation barrier approaches a *constant*  $U_{max}$ . Upon using the one-dimensional version of Eq. (62), we find that the prefactor of the Arrhenius exponential term  $e^{-U_{max}/T}$  is proportional to  $\sqrt{U''(x_{max})}$ , which vanishes as  $\sigma_{xy} \rightarrow 0$  and the maxima becomes shallower. Using Eq. (31) we find that in this case the prefactor vanishes as  $\sqrt{\sigma_{xy}}$ , up to logarithmic corrections, so that:

$$\Gamma \propto \sqrt{\sigma_{xy}} e^{-U_{max}/T}. \quad (73)$$

The above calculation represents a special case, since two antiparallel dislocations with Burgers vectors making a generic, finite angle with the  $\hat{x}$  direction (say,  $\theta$  and  $\theta - \pi$ ), will have an interaction that provides a term *linear* in  $x$  for  $x \gg W$ . Using Eq. (37) and Eqs. (11) we find that the component of the interaction force in the glide direction is:

$$F_{int} = 2\pi Ab^2 \cos(\theta) \sin(\theta)/W \quad (74)$$

A  $\sigma_{xy}$  twist stress imposed on the boundaries of the cylinder results in a force which has a component in the glide direction. Using Eqs. (9) and (12) we find that:

$$F_g = F_x \cos(\theta) + F_y \sin(\theta) = b\sigma_{xy}[\cos^2(\theta) - \sin^2(\theta)]. \quad (75)$$

Thus, there will be a critical  $\sigma_{xy}^*$  for which the interaction term is compensated by the external stress, i.e.,  $F_g = F_{int}$ :

$$\sigma_{xy}^* = \frac{2\pi Ab}{W} \tan(2\theta). \quad (76)$$

At very low temperatures, the dislocations would no longer be able to surmount the Peierls potential barriers. Then, the two dislocations will glide away from each only for a much larger stress,  $\sigma_{xy} \sim A$ , for which the force due to the external stress overcomes the periodic Peierls potential [4]. At finite temperature and  $\sigma_{xy} > \sigma_{xy}^*$ , we obtain a similar escape-of-a-barrier problem we had in the previous case, which can be solved in a similar manner. In this case, however, the glide direction forms an angle  $\theta$  with the  $\hat{x}$ -axis, and once the dislocations unbind they make a helical trajectory along to the glide direction.

### ACKNOWLEDGMENTS

We thank B. I. Halperin, W. T. M Irvine, F. Spaepen and V. Vitelli for useful discussions. This work was supported by the National Science Foundation via Grant DMR1005289 and through the Harvard Materials Research Science and Engineering Laboratory, through Grant DMR0820484. A.A. was supported by a Junior Fellowship of the Harvard Society of Fellows.

### The Airy stress function for a cylinder

For some applications, it is convenient to describe the elastic stresses in terms of the Airy stress function  $\chi$ , defined by  $\sigma_{ij}(\vec{r}) = \epsilon_{im}\epsilon_{jn}\partial_m\partial_n\chi(\vec{r})$ , which is a solution of the bi-harmonic equation [4, 18]. For a set of dislocations  $\{\vec{b}_\alpha\}$  located at positions  $\{\vec{r}_\alpha\}$  with zero external stress, the Airy function satisfies [43]:

$$\nabla^2\chi(\vec{r}) = 4\pi A \sum_{\alpha} \epsilon_{ij} b_{\alpha i} \partial_j \delta(\vec{r} - \vec{r}_\alpha). \quad (77)$$

We can obtain  $\chi(x, y)$  from the strains, via:  $\frac{\partial^2\chi}{\partial x^2} = \sigma_{yy}$ ,  $\frac{\partial^2\chi}{\partial x^2} = \sigma_{yy}$ ,  $\frac{\partial^2\chi}{\partial x\partial y} = -\sigma_{xy}$ . Since for a dislocation with

$\vec{b} = b\hat{x}$ ,  $b\sigma_{xy}^x = \frac{\partial E_{x,-x}}{\partial x} = -b\frac{\partial^2 \chi^x}{\partial x \partial y}$  and  $-b\sigma_{xx}^x = \frac{\partial E_{x,-\hat{x}}}{\partial y} = -b\frac{\partial^2 \chi^x}{\partial^2 y}$ , we find:

$$\frac{\partial \chi_x}{\partial y} = -(1/b)E_{\hat{x},-\hat{x}}(x,y). \quad (78)$$

Upon integration this leads to:

$$\begin{aligned} \chi^x(x,y) = & \frac{Ab}{2W} \{ \pi xy - xW \arctan[\cot(\pi y/W) \tanh(\pi x/W)] \\ & + (ix+y)W \log \left[ 1 - e^{2\pi(iy-x)/W} \right] \} \\ & - \frac{Aby}{2} (y+ix) \log[\sinh[\pi(x-iy)/W]] \\ & - \frac{AbW}{4\pi} \left( i \text{PolyLog} \left[ 2, e^{-2\pi(x-iy)/W} \right] \right) + C.C. \end{aligned} \quad (79)$$

Although one could add an undetermined function  $G(x)$  to this expansion, the derivatives of  $\chi^x$  with  $G(x) = 0$  satisfy the above equations, and thus Eq. (79) is the desired solution.

Similarly, for a dislocation with  $\vec{b} = b\hat{y}$ , we find:

$$\frac{\partial \chi_y}{\partial x} = (1/b)E_{\hat{y},-\hat{y}}(x,y), \quad (81)$$

which upon integration leads to:

$$\begin{aligned} \chi^y(x,y) = & \frac{-iAby}{2} \{ \text{Log} \left[ 1 - e^{-2\pi(x-iy)/W} \right] \\ & + \text{Log}(i \text{Sinh}[\pi(x+iy)/W]) \} \\ & - \frac{Abe^{-i\pi y/W} (-i + \text{Tan}[\pi y/W])}{4 \text{Sec}[\pi y/W]} \{ y \text{Log} \left[ 1 - e^{-2\pi(x-iy)/W} \right] \\ & (-ix+y) \text{Log}[\text{Sinh}[\pi(x+iy)/W]] \} + C.C. \end{aligned} \quad (82)$$

Although adding an undetermined function  $H(y)$  is again possible, one can check that for  $H(y) = 0$  we have  $\frac{\partial \chi_y}{\partial x^2}(x,y) = \sigma_{yy}$ ,  $\frac{\partial \chi_y}{\partial y^2}(x,y) = \sigma_{xx}$ ,  $\frac{\partial \chi_y}{\partial x \partial y}(x,y) = -\sigma_{xy}$ , as required.

### Affine deformations of crystals on a cylinder

Consider a lattice on a cylinder defined by minimal unit basis vectors  $\hat{e}_1$  and  $\hat{e}_2$ . As discussed in section , the lattice can be characterized by a pair of integers  $(M, N)$  such that:

$$Mb\hat{e}_1 + Nb\hat{e}_2 = W\hat{y}. \quad (83)$$

Upon neglecting uniform translations, a general affine deformation of this lattice can be written as:

$$\begin{aligned} u_x(x,y) &= \alpha_{xx}x + \alpha_{xy}y \\ u_y(x,y) &= \alpha_{yx}x + \alpha_{yy}y. \end{aligned} \quad (84)$$

These displacements will also result in a crystal, characterized by different unit vectors  $\hat{g}_1$  and  $\hat{g}_2$ . The actual values of the matrix  $\alpha$  will be determined by boundary conditions, such as counter-rotating twists applied to the ends of the cylinder. In general, the deformation matrix will not be symmetrical, although (neglecting a weak dependence of the lattice orientation relative to the cylinder axis), the energy has to be independent of the antisymmetric part  $\frac{1}{2}(\alpha_{xy} - \alpha_{yx})$ . From the periodicity in the  $y$  direction we find that:

$$u_x(x,y+W) = u_x(x,y) + b(m\hat{g}_1 + n\hat{g}_2), \quad (85)$$

where  $m$  and  $n$  are integers, leading to:

$$\alpha_{xy} = \frac{b}{W}(m\hat{g}_{1,x} + n\hat{g}_{2,x}), \alpha_{yy} = \frac{b}{W}(m\hat{g}_{1,y} + n\hat{g}_{2,y}). \quad (86)$$

Note that for small stresses corresponding to integers  $m, n$  which are not too large, we can replace the basis vectors  $\hat{g}_1$  and  $\hat{g}_2$  by  $\hat{e}_1$  and  $\hat{e}_2$ , up to corrections of order  $(b/W)^2$ , which is a higher order effect.

From Eq. (86) we conclude that the components of the deformation tensor  $\alpha_{xy}$  and  $\alpha_{yy}$  are quantized on a cylinder, while the components  $\alpha_{xx}$  and  $\alpha_{yx}$  are *not* quantized. Considering the strain matrix  $u_{ij} = \frac{1}{2}(\partial_i u_j + \partial_j u_i)$ , we find that  $u_{xx} = \alpha_{xx}$  is *not* quantized, since we have no restrictions on  $u_x$ , while  $u_{yy} = \alpha_{yy}$  is quantized. The off-diagonal component  $u_{xy} = \frac{1}{2}(\alpha_{xy} + \alpha_{yx})$  is a combination of a quantized object and a non-quantized object, and is thus *non*-quantized. The stress tensor is related to the strain tensor via the relation:

$$\sigma_{ij} = 2\mu u_{ij} + \lambda \delta_{ij} u_{kk}. \quad (87)$$

Each of the components of the stress tensor has a non-quantized piece. Thus, the Peach-Koehler stress is fact non-quantized. Note, however, that *particular* linear combinations of the stress tensor components can be quantized, similar to the case of superfluid films on cylinders [11, 44].

[1] E. Orowan, Z. Phys. **89**, 605 (1934).

[2] G. I. Taylor, Proc. R. Soc. (London) Ser. A **145**, pp. 362 (1934).

[3] J. M. Burgers, Proceedings of the Physical Society **52**, 23 (1940).

- [4] J. P. Hirth and J. Lothe, *Theory of Dislocations* (Wiley, New York, 1982).
- [5] D. R. Nelson and B. I. Halperin, Phys. Rev. B **19**, 2457 (1979).
- [6] W. T. M. Irvine, V. Vitelli, and P. M. Chaikin, Nature **468**, 947 (2011).
- [7] R. Gillette and D. Dyson, The Chemical Engineering Journal **2**, 44 (1971).
- [8] D. R. Nelson, Annual Review of Biophysics **41**, 371 (2012).
- [9] A. Amir and D. R. Nelson, PNAS **109**, 9833 (2012).
- [10] H. Lamb, *Hydrodynamics* (Dover, New York, 1945).
- [11] J. Machta and R. A. Guyer, J. Low Temp. Phys. **74**, 231 (1989).
- [12] J. Langer, Annals of Physics **54**, 258 (1969).
- [13] W. Coffey, Y. P. Kalmykov, and J. T. Waldron, *The Langevin Equation* (World Scientific, Singapore, 1996).
- [14] K. D. Young, Annual Review of Microbiology **64**, 223 (2010).
- [15] S. Takeuchi, W. R. DiLuzio, D. B. Weibel, and G. M. Whitesides, Nano Letters **5**, 1819 (2005).
- [16] D.-J. Scheffers and M. G. Pinho, Microbiology and Molecular Biology Reviews **69**, 585 (2005).
- [17] See, e.g., S. Ostlund and B. I. Halperin, Phys. Rev. B **23**, 335 (1981).
- [18] L. D. Landau and E. M. Lifshitz, *Elasticity Theory* (Pergamon, Princeton, 1986).
- [19] A. R. Bausch, M. J. Bowick, A. Cacciuto, A. D. Dinsmore, M. F. Hsu, D. R. Nelson, M. G. Nikolaides, A. Travesset, and D. A. Weitz, Science **299**, 1716 (2003).
- [20] H. S. Seung and D. R. Nelson, Phys. Rev. A **38**, 1005 (1988).
- [21] See, for example, R. D. Kamien, D. R. Nelson, C. D. Santangelo, and V. Vitelli, Phys. Rev. E **80**, 051703 (2009).
- [22] H. W. Lee and L. S. Levitov, *Symmetry in Plants* (World Scientific, Singapore, 1998).
- [23] C. Kuhlemeier, Trends in Plant Science **12**, 143 (2007).
- [24] R. O. Erickson, Science **181**, 705 (1973).
- [25] C. R. Calladine, Nature **255**, 121 (1975).
- [26] G. B. Olson and H. Hartman, J. Phys. (Paris), Colloq. **43**, C4 (1982).
- [27] L. S. Levitov, Phys. Rev. Lett. **66**, 224 (1991).
- [28] C. Nisoli, N. M. Gabor, P. E. Lammert, J. D. Maynard, and V. H. Crespi, Phys. Rev. Lett. **102**, 186103 (2009).
- [29] C. Nisoli, N. M. Gabor, P. E. Lammert, J. D. Maynard, and V. H. Crespi, Phys. Rev. E **81**, 046107 (2010).
- [30] A. Mughal, H. K. Chan, and D. Weaire, Phys. Rev. Lett. **106**, 115704 (2011).
- [31] N. C. Darnton and H. C. Berg, Biophysical journal **92**, 2230 (2007).
- [32] S. Maki-Yonekura, K. Yonekura, and K. Namba, Nature structural & molecular biology **17**, 417 (2010).
- [33] M. Peach and J. S. Koehler, Phys. Rev. **80**, 436 (1950).
- [34] J. Weertman (Phil. Mag. **11**, 1217 (1965)) has suggested that only the *traceless* part of the stress tensor should enter Eq. (8), a view which also appears in recent editions of Ref. [18]. Here, however, we take the more conventional perspective of Lothe and Hirth (J. App. Phys. **38**, 845 (1967)), which we believe is the appropriate one for cylindrical geometries where new material is supplied from the bulk for the climb process.
- [35] J. Weertman, Philosophical Magazine **11**, 1217 (1965).
- [36] See, e.g., J. Mathews and R. L. Walker, Mathematical Methods of Physics (W. A. Benjamin, Inc., New York, 1964).
- [37] For a careful discussion of how to extract dislocation core energies from the large distance energetics of dislocation pairs see: D. S. Fisher, B. I. Halperin and R. Morf, Phys. Rev. B. **20**, 4692 (1979).
- [38] R. Bruinsma, B. I. Halperin, and A. Zippelius, Phys. Rev. B **25**, 579 (1982).
- [39] S. Wang, L. Furchtgott, K. C. Huang, and J. W. Shaevitz, PNAS **109**, E595 (2012).
- [40] A.A. is indebted to W. T. M. Irvine for useful discussions of this point.
- [41] V. Ambegaokar, B. I. Halperin, D. R. Nelson, and E. D. Siggia, Phys. Rev. B **21**, 1806 (1980).
- [42] A. Zippelius, B. I. Halperin, and D. R. Nelson, Phys. Rev. B **22**, 2514 (1980).
- [43] D. R. Nelson, *Defects and Geometry in Condensed Matter Physics* (Cambridge Univ. Press, Cambridge, 2002).
- [44] D. R. Nelson and A. Amir, to be published.